COMPUTER STUDIES OF THE DYNAMIC STRENGTH OF CERAMICS

D. Steinberg

▶ **To cite this version:**

D. Steinberg. COMPUTER STUDIES OF THE DYNAMIC STRENGTH OF CERAMICS. Journal de Physique IV Proceedings, 1991, 01 (C3), pp.C3-837-C3-844. 10.1051/jp4:19913117 . jpa-00249920

HAL Id: jpa-00249920
https://hal.science/jpa-00249920

Submitted on 4 Feb 2008

HAL is a multi-disciplinary open access archive for the deposit and dissemination of scientific research documents, whether they are published or not. The documents may come from teaching and research institutions in France or abroad, or from public or private research centers.

L'archive ouverte pluridisciplinaire **HAL**, est destinée au dépôt et à la diffusion de documents scientifiques de niveau recherche, publiés ou non, émanant des établissements d'enseignement et de recherche français ou étrangers, des laboratoires publics ou privés.

JOURNAL DE PHYSIQUE IV C3-837
Colloque C3, suppl. au Journal de Physique III, Vol. 1, octobre 1991

COMPUTER STUDIES OF THE DYNAMIC STRENGTH OF CERAMICS

D.J. STEINBERG

Lawrence Livermore National Laboratory, P.O. Box 808 (L35), Livermore, CA 94551, U.S.A

Des simulations numériques de la résistance dynamique de six céramiques sont effectuées avec une nouvelle loi de comportement. L'influence des déformation, vitesse de déformation, pression, température et effet Bauschinger est montrée en déterminant le temps de réponse des céramiques aux grandes vitessses de sollicitation. La loi de comportement est facile à implanter dans un code hydrodynamique et reproduit correctement le comportement de ces matériaux.

Abstract Using a new constitutive model, computer studies were performed concerning the dynamic yield strength of six ceramics, SiC, TiB_2, AlN, two types of B_4C, and partially stabilized zirconia. The relative importance of the thermomechanical variables, strain, strain-rate, pressure, and temperature, as well as the Bauschinger effect, is demonstrated in determining the time response of ceramics to high-strain-rate deformation. The constitutive model is easy to implement in a hydrodynamic computer code and successfully reproduces a variety of data for these materials.

1.– Introduction

The high-strain-rate behavior of ceramics offers exciting scientific possibilities, for these materials appear to have more individual peculiarities than do metals. In the case of metals, a large experimental data base exists that permitted us to construct a constitutive model by using principally non-shock-wave sources /1,2/. We then used shock-induced, time-resolved wave profiles to test the predictive capability of the model. These experiments are excellent and stringent tests of any model because so many thermomechanical effects take place simultaneously. Hydrodynamic computer-code calculations using this model were very successful in simulating the experimental results. For ceramics, we are not so fortunate. Because of the dearth of data, it is neccessary to use shock-wave profiles as a primary source of of material-response information.

I chose six materials to study: SiC, two types of B_4C, AlN, TiB_2, and ZrO_2, partially stabilized with 3 wt.% Yttria in the tetragonal form (PSZ). All materials were near their theoretical density. Regardless of the actual micromechanical mechanisms, I have assumed that all thermomechanical behavior can be represented through the following macroscopic variables: strain ε, strain rate $\dot{\varepsilon}$, temperature T, and pressure P. Furthermore, strain is not used except for the special case of B_4C. This is because plastic strains are typically only a few percent and also because the Bauschinger effect appears to be small.

The simplest form of the Cochran-Guinan Bauschinger model is used throughout because I believe it is a better general representation of reality than is simple elastic-plastic behavior /1/. I have also used the spall model of Cochran and Banner with a spall strength of 1 GPa /3/. Because spall strengths relative to yield strengths for ceramics are small and the peak stresses in the experiments exceed 20 GPa, it is, in any case, difficult to quantify spall in these studies.

The hydrodynamic equation of state used in this study is the Mie-Grüneisen equation with a nonlinear shock velocity–particle velocity (U_s–U_p) relationship,

$$U_s = C_0 + S_1 U_p + S_2 \left(\frac{U_p}{U_s}\right) U_p + S_3 \left(\frac{U_p}{U_s}\right)^2 U_p \ , \qquad (1)$$

Article published online by EDP Sciences and available at http://dx.doi.org/10.1051/jp4:19913117

and $\gamma\eta$ equal to a constant, γ_0, where γ is Grüneisen's gamma, and η denotes compression. Table 1 gives all the required material parameters. In this table, ρ_0 is the initial density, C_0 is the bulk sound speed, and S_{1-3} are the slope parameters of the Hugoniot. A more complete discussion of this work can be found in ref. /4/.

Table 1. Material Parameters .

Material	ρ_0 (g/cm^3)	C_0 (mm/μs)	S_1	γ_0	G_0 (GPa)	Y_A (GPa)	A (TPa^{-1})	A(est) (TPa^{-1})	B(est) (10^{-4} K^{-1})	D (MPa-s^n)	D(est) (MPa-s$^{1/3}$)	K_{IC} (MPa-m$^{1/2}$)
SiC	3.177	8.19	0.88	1.16	186.9	12.0	12	12	1.0	120	12	4.4
PSZ	6.028	5.67	1.0*	1.57	83.4	6.0	30	16	3.4	12	19	8.25
B_4C (E-P)	2.516	9.57	1.0	1.46	199.3	11.1	11	14	3.0	36	7.5	2.4
(Dow)	2.506	9.65			197.2	12.1						
TiB_2	4.452	6.96	5.288	1.39	237.2	4.8/10.1	12.	14.5	1.0	36	13	4.6
AlN	3.26	7.83		1.34	130.			15	1.5	12	12	4.5

1. n is always 0.366. 2. For SiC, Y_L = 1.9 Gpa. 3. For TiB_2, B (meas.) = 0.94×10^{-4}; $S_2 = -2.6$, $S_3 = 71.3$.
4. For B_4C, C = 0.88 eV (E-P) and 1.21 eV (Dow); C(est) = 0.7–1.1 eV. *Estimated.

2.– Constitutive Model

The shear modulus G is the same form as for metals /1/.

$$G(P,T) = G_0\left[1 + A\frac{P}{\eta^{1/3}} - B(\Delta T)\right] . \qquad (2)$$

Here, $\Delta T = T - 300$ K, subscript 0 refers to the initial state ($P = 0$ and $T = 300$ K), and coefficients A and B are material-dependent parameters: $A = 1/G_0(dG/dP)$, and $B = 1/G_o(dG/dT)$.

For metals, a wealth of data exists for A and B. Unfortunately, almost no such data exist for ceramics. To estimate A, I used a relationship, derived originally for metals, from Guinan and Steinberg /5/. This requires a knowledge of the STP elastic constants, γ_0 and the Hugoniot . Values for A(est) are given in Table 1, as are the values of A used in simulating the wave profiles. Except for PSZ, A and A(est) agree well.

Because the temperature effect is usually very small for metals, I wanted to see if this was also the case for ceramics. I again used the results of Guinan and Steinberg to estimate B /5/. Some data exist for the temperature derivative of Young's modulus for all five ceramics. This information plus the STP elastic constants, the Hugoniot, and the volume thermal expansion coefficient provide the necessary data to determine B(est). These results are given in Table 1. Only for TiB_2 has B been measured /6/, and the result is in very good agreement with B(est). Calculations of the wave profiles were done, including the temperature effect, with the result that ceramic behavior was very similar to that of metals; i.e., the temperature effect was about an order of magnitude less important than the effect of pressure, or barely discernible compared with experimental uncertainty.

Grady /7,8/ has developed a model for the brittle fracture stress σ_c vs $\dot{\varepsilon}$ for brittle materials in tension that appears to hold experimentally for the yield strength Y in compression as well /9,10/: $\sigma_c = D\,\dot{\varepsilon}^n$, where $D = (3\rho_0 C_0 K_{IC}^2)^n$, and K_{IC} is the critical stress intensity factor. In Grady's work, n is 1/3. However, Grady has noted that there is no reason why n could not be larger or smaller than this value. To help determine D and n, there are also the data of Lankford for Y vs $\dot{\varepsilon}$ for SiC /9,11/, PSZ /10/, and AlN (unpublished data). These data are shown in Fig. 1. At static conditions, one set of data for SiC was 0.7 GPa lower than the other. I added 0.7 GPa to this set because it is the shape of the Y vs $\dot{\varepsilon}$ curve that is of interest here. With n = 0.366 in all cases, these data were fit to within the experimental uncertainty by using the values of D given in Table 1. Lankford has said that the absolute error for the data at $\dot{\varepsilon} = 10^3$ s^{-1} is about 20 to 30%. Table 1 also gives values for D(est) based on Grady's model. Here, n must be 1/3 to be dimensionally correct. For PSZ and AlN, D and D(est) are in remarkable agreement, but for SiC, D exceeds D(est) by an order of magnitude.

The yield strength is assumed to be a sum of strain-rate–dependent and strain-rate–independent terms similar to our approach for metals /2/. In addition, both terms are multiplied by the normalized shear modulus. This scaling of Y on G is also the same as we have done for metals /1/:

$$Y = (D\,\dot{\varepsilon}^n + Y_A)\,G(P,T)/G_0 . \qquad (3)$$

Here, Y_A is a material constant that can be sample dependent, as it is a function of purity, grain-size, previous mechanical history, etc. Finally, the rate-dependent part of Y is limited, i.e., $D\,\dot{\varepsilon}^n \le Y_L$. The yield strength cannot increase without limit as $\dot{\varepsilon}$ increases. We know, for example, that the Hugoniot elastic limit (HEL) does not increase as a material is shocked to higher and higher stress. The limit on $\dot{\varepsilon}$ effects, Y_L, should therefore be the difference between the yield strength at the HEL and Y_A. The effect of Y_L on the calculations is evident only when Y increases very rapidly with $\dot{\varepsilon}$ (i.e., D is large) and the peak stress is very high. Such is the case only for SiC, where Y_L = 1.9 GPa.

The VISAR records for SiC and PSZ have been normalized to the calculations at peak velocity. Only for PSZ does this normalization exceed the absolute error of the VISAR.

3.– Results and Discussion

SiC

Three shock-wave–profile experiments for SiC, done by Kipp and Grady (/12/ and unpublished data) are compared with the computer simulations in Figs. 2 through 4. Additional results are tabulated in Tables 2 and 3. Figure 2 shows the effect of removing the rate dependence. The shape of the loading curve is now totally wrong. The simulation of these experiments is remarkably sensitive to the value of n. Originally, I tried keeping $n = 1/3$ but failed to get simulations that agreed well with the data. Increasing n by only 10% to 0.366 solved the problem. Apparently, the shape of the shock-loading curve is a more sensitive measure of rate effects than are Hopkinson split bar experiments.

The effect of removing Y_L (i.e., Y_L is infinite) is illustrated in Fig. 3. It is apparent that the use of Y_L sharpens the shock front, in agreement with the data, but even so, it hardly plays a dominant or decisive role in the calculations. Figure 4 shows what happens if the pressure dependence is removed. Because the total energy in the system does not change, the biggest difference is in timing, not amplitude. The poor agreement now in release time shows that the value for A(est) was very good. Removing the P and $\dot{\epsilon}$ effects from the model also makes the calculated amplitude of the elastic reflection on loading too low.

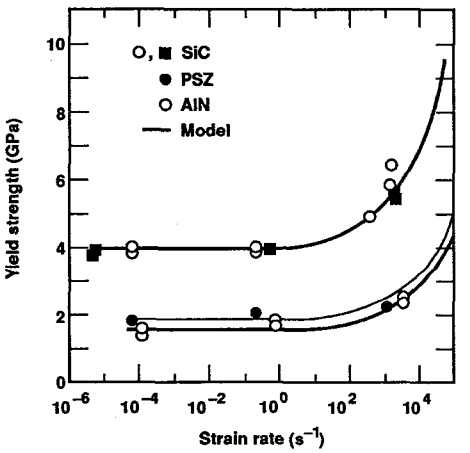

Fig. 1. Yield strength vs strain rate. Comparison of the model and the data.

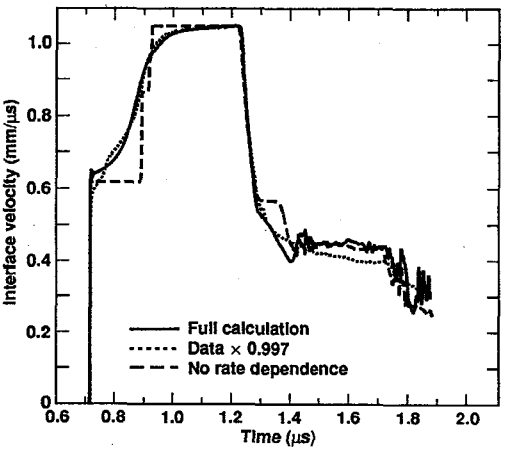

Fig. 2. Comparison of calculation and the low-stress experiment for SiC with and without rate dependence.

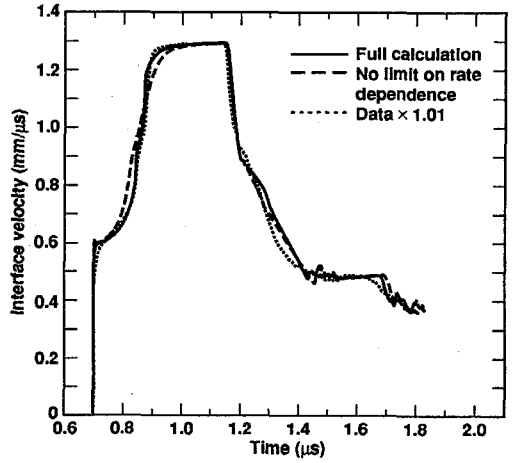

Fig. 3. Comparison of calculation and the middle-stress experiment for SiC with and without the rate-dependent limit.

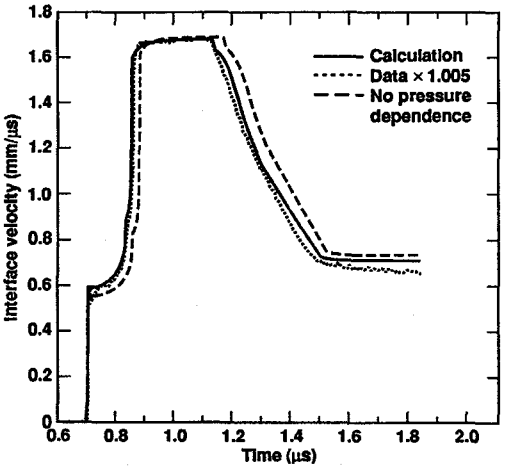

Fig. 4. Comparison of calculation and the high-stress experiment for SiC with and without pressure dependence.

Table 2. Calculated values of the Hugoniot elastic limits.

Material	HEL (GPa)
SiC	17.4
PSZ	16.2
B_4C (Dow)	16.9
B_4C (Eagle-Picher)	15.4
TiB_2 (low)	6.2
TiB_2 (high)	13.8

Table 3. Calculated peak values of various thermomechanical variables.

Sandia ID	Material	σ (GPa)	P (GPa)	T (K)	ε (%)	$\dot{\varepsilon}$ (s^{-1})	Y (GPa)
CE4	SiC	27.2	17.4	506	2.35	1.3×10^4	16.0
CE5	SiC	36.1	25.7	674	4.2	7.8×10^4	17.0
CE31	SiC	48.9	37.7	930	6.7	1.7×10^5	18.4
CE22	PSZ	28.8	22.3	464	3.1	8.0×10^3	10.7
CE7	TiB_2 (low)	47.9	43.1	556	6.2	5.5×10^4	10.4
CE3	B_4C (E.P.)	22.9	18.8	476	3.7	5.2×10^3	6.1*
CE6	B_4C (E.P.)	32.0	28.7	579	6.0	2.0×10^4	5.0*
CE17	B_4C (Dow)	23.9	20.9	502	4.35	1.0×10^4	4.4*
CE18	B_4C (Dow)	29.9	27.5	569	5.85	2.25×10^4	3.7*

*Y at σ_{max}.

Figure 5 shows Y as a function of time for all three experiments. The increase in Y is caused by the increase in P and $\dot{\varepsilon}$. For the low-stress experiment, the effects of these parameters at the maximum Y are about equal, but for the high-stress experiment, the effect of $\dot{\varepsilon}$ is only about 30% of the total.

PSZ

Grady has provided me with one unpublished wave profile for PSZ, in which the peak stress is below the transition to the monoclinic phase. Figure 6 compares the simulation and data, and the overall agreement is good. In particular, the calculated shape of the shock-loading curve agrees well with the experiment. For PSZ, then, the wave-profile data, Lankford's data, and Grady's model for Y vs $\dot{\varepsilon}$ are all in very good agreement. At the maximum value of Y, the effect of pressure accounts for about 2/3 of the increase and rate effects about 1/3.

The parameter A differs significantly from A(est). PSZ has a tetragonal crystal structure, and tetragonal metals are known to have large values of A. However, for metals, A is proportional to γ_0, and tetragonal metals have large values of γ_0, quite unlike PSZ. This points out the crucial importance of measuring $G(P)$.

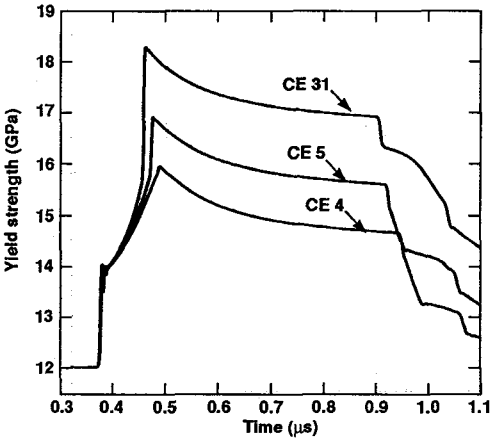

Fig. 5. Calculated yield strength vs time at the center of the target for the three SiC experiments.

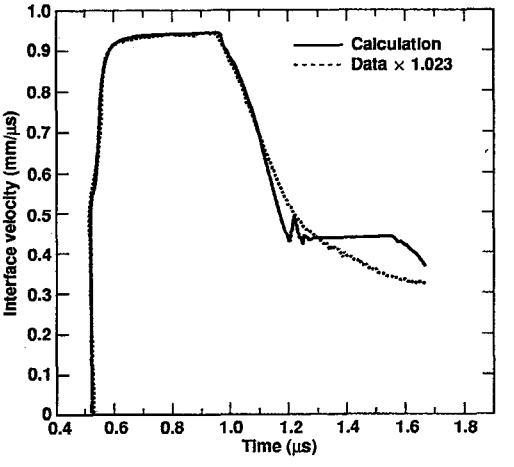

Fig. 6. Comparison of calculation and experiment for PSZ.

B_4C

The data for B_4C show several unusual characteristics (see Figs. 7–10). The first are the sharp oscillations with a frequency of a few tens of nanoseconds. M. Guinan of Lawrence Livermore Laboratory has suggested that these observations could be explained if there is elastic precursor decay. This is not the decay of the leading edge of the wave as it passes through a material; rather, at any time, the strength of the wave is greatest at its leading edge and gradually falls off behind the leading edge. This is reminiscent of a Taylor wave in high explosives. When the precursor reflects from the lower-impedance LiF window, it will see a progressively lower elastic stress as it moves back into the shocked material. If the difference between the release wave and the oncoming part of the elastic wave exceeds the spall strength of the material, then a gap or gaps can open, and the measured velocity will drop. As these waves and the main shock wave continue to interact, these gaps can be closed and reopened, causing the signal to alternately rise and fall until the main shock finally closes them. More structure exists in the data for the Dow material than for the Eagle-Picher material. This is because there is more time between the elastic and plastic waves for the former, allowing more wave interactions. This is consistent with the higher HEL for the Dow material, and hence the shallower Rayleigh line.

Figure 7 shows only the calculated loading curve with no rate dependence for experiment CE3. This calculation was done to clearly delineate the many wave interactions and how they correlate with the data. In particular, note the calculated increase at $t = 1.04$ μs and how well it corresponds with the abrupt change from a decreasing to an increasing velocity in the data. I believe that this is the most striking example of wave interactions—in this case, the closing of a spall-induced gap as a result of the arrival of a new shock reverberation. In Fig. 9, the stress corresponding to the sharp peak at the HEL is 20.7 GPa. This exceeds by 4.6 GPa the stress corresponding to the minimum in velocity that follows about 50 ns later. This drop in stress far exceeds the measured spall stress in B_4C (D. Grady, Sandia National Laboratories, unpublished data), which also agrees with the precursor decay hypothesis. However, no attempt is made in this paper to actually calculate these oscillations.

Another unusual characteristic of the wave profiles is the very long time between the arrivals of the elastic and plastic waves. Simple elastic-plastic behavior, with a constant offset between the Hugoniot and the hydrostat, would imply a very much smaller time difference. This behavior is also shown in the Hugoniot data of Gust and Royce /13/ in Fig. 10. Just above the HEL, the slope of the Rayleigh line becomes very shallow, implying a very low shock speed relative to the elastic-wave speed. The four arrows in Fig. 10 point to where the four wave-profile experiments fall on this Hugoniot.

Other unusual properties of boron-rich compounds have been described by Emin /14/. The crystal structure of B_4C is highly unusual. The basic structure is rhombohedral, with an icosahedral structure unit occupying each vertex of the rhombohedron. According to Emin, the space inside each icosahedron is large enough to hold a magnesium ion. I believe that these icosahedra collapse under the influence of a strong shock, which is the cause of the sudden drop in the material strength. To accomplish this reduction, I have replaced Y_A by $Y_A \exp(-C\varepsilon/kT)$, where k is Boltzmann's constant and C is a material-dependent parameter. A number of estimates of the activation energy C were made with the result that C(est) lies between 0.7 and 1.1 eV. These estimates are in reasonable agreement with the values of C used in the calculations.

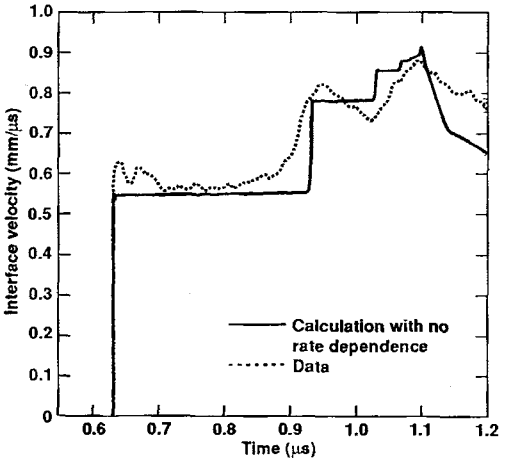

Fig. 7. Comparison of a rate-independent calculation and Sandia experiment CE3 for B_4C.

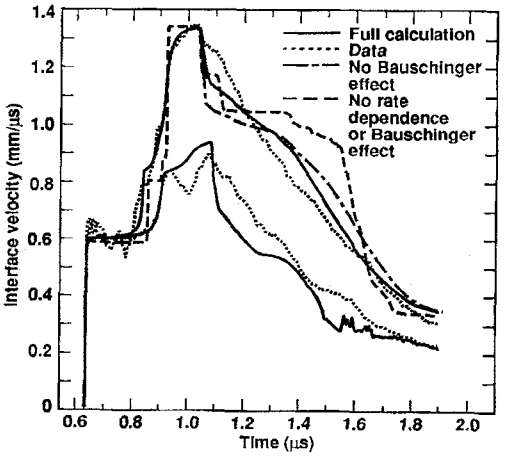

Fig. 8. Comparison of calculation and data for two B_4C experiments using Eagle-Picher material.

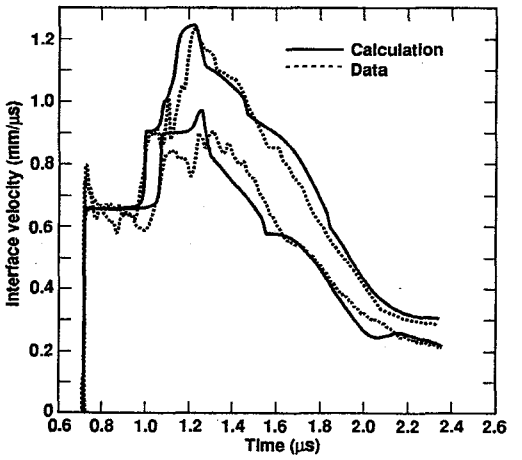

Fig. 9. Comparison of calculation and data for two B_4C experiments using Dow material.

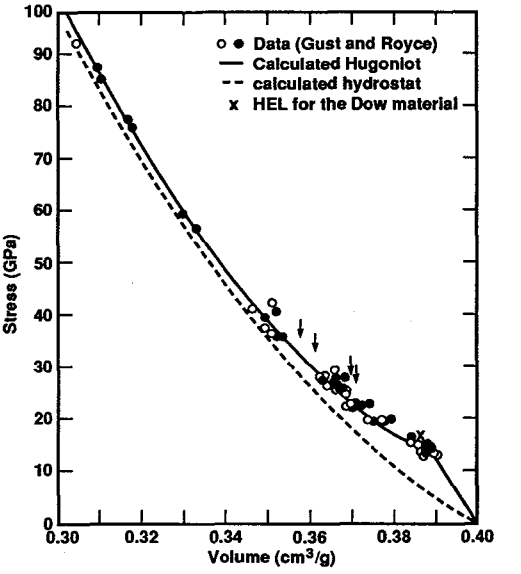

Fig. 10. Comparison of the calculated Hugoniot with the data for B_4C. Also shown is the calculated hydrostat. The arrows point to where the four wave-profile experiments fall on the Hugoniot.

The low-stress experiment for the Eagle-Picher material was used to normalize the code. The parameters A, C, D, and Y_A were adjusted to give the best calculational agreement with the data. As before, A was chosen to reproduce the arrival time of the elastic release, and Y_A was adjusted to give the observed HEL. Because there are no Y vs $\dot{\varepsilon}$ data, D was adjusted to give the observed slope of the wave profile at the first elastic reflection. Finally, C was adjusted so that this elastic reflection arrived at the observed time. While A and A(est) are in good agreement, D and D(est) disagree by a factor of about 5. Figure 8 compares this adjusted calculation and the data. A good test of the model is now to calculate the higher-pressure experiment by using the same parameters. This comparison is also shown in Fig. 8. The agreement is remarkably good. Note that all the elastic reflections arrive at the correct time on shock loading. The agreement on release is excellent; the code correctly calculates the gradual falloff of the signal.

Using the same values of A and D, I adjusted C and Y_A again to fit the low-stress experiment for the Dow material, which appears to have an HEL that is about 10% higher than the Eagle-Picher material. Because of this, the time difference between the elastic and plastic waves is greater. Therefore, C for this material is also greater than for the Eagle-Picher material. The comparison of experiment and calculation is shown in Fig. 9. The agreement is good, even for the release wave. As was done for the first material, the higher-stress experiment was used to test the model. This comparison is also shown in Fig. 9. The agreement is excellent. Again, all the timing is correctly reproduced, as is the gradually sloping release curve.

An additional test of the model is to compare a set of calculated Hugoniot final states with the data of Gust and Royce /13/. These results are shown in Fig. 10 for the Eagle-Picher material. The solid line is the calculated locus of Hugoniot states, and it is in excellent agreement with the data both above and below the stress levels corresponding to the measured wave profiles. An interesting result of the calculations is that above about 35 GPa, the calculated ratio of ε/T is roughly constant. This implies that Y does not approach zero, but rather remains at a constant value—about 30% of the value at the HEL for the Dow material and about 45% of the value for the Eagle-Picher material.

Figure 8 illustrates the importance of rate effects and the Bauschinger model as they affect the release curve. In this figure are shown calculations (1) without the Bauschinger model and (2) without either the rate effects or the Bauschinger model. It is quite evident that both play a role in smoothing and shaping the release curve. Along with Figs. 2 and 4, these computer studies show how all parts of this model work together to shape the calculated the wave profiles.

TiB_2

TiB_2 has a number of unusual properties. Based on their Hugoniot data, Gust, Holt, and Royce /15/ have suggested a possible phase transition at 30 GPa (see Fig. 11). In addition, all the shock-wave–profile data from Sandia (/12/ and unpublished data) show two breaks in the loading profiles at stresses of about 6 and 13.5 GPa (see Fig. 12). These have been variously referred to as a "double-yield" or yield plus phase transition. Finally, the shear modulus is greater than the bulk modulus.

The Hugoniot data of Gust, Holt, and Royce /15/ and the bulk sound speed of Kipp and Grady /12/ were fitted by using Eq. (1). This fit is shown in Fig. 11, in which the slight oscillation is an artifact of the fit only. The arrow at U_p = 1.05 mm/μs shows where the experiment of Kipp and Grady would fall. Because no Y-vs -$\dot{\epsilon}$ data exist, D was merely adjusted to give the best fit to the slope and shape of the shock-loading curve; it is about a factor of 3 higher than D(est). Figure 12 compares the wave-profile experiment with two calculations, each assuming the different values of the HEL. The agreement between experiment and calculation is reasonable, but certain features related to the double-yield obviously will not be reproduced. More work is certainly needed here.

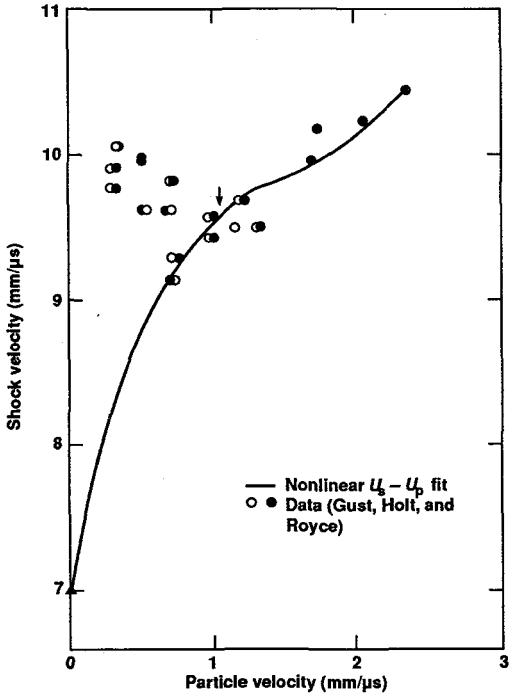

Fig. 11. Hugoniot data for TiB_2 and the nonlinear U_S–U_P fit. The arrow shows where the experiment of Kipp and Grady would fall.

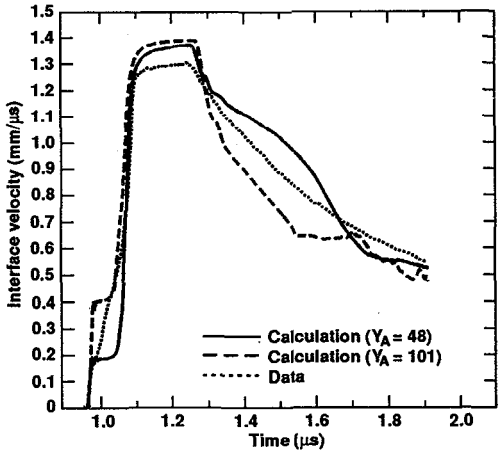

Fig. 12. Comparison of calculation and experiment for TiB_2 for both high and low HEL.

4.– Conclusions

The majority of the work presented is for two carbides that could not be more different. SiC, with its large thermal conductivity, appears to be rather metal-like. On the other hand, B_4C is probably as exotic a material as one can find, and quite unlike SiC. TiB_2 has interesting structures in its wave profiles that are not understood. In addition, at least four different crystal structures are represented. In spite of these differences, certain themes seem to run throughout all the studies. One is the importance of pressure and strain rate in determining the yield strength. While this point has been made by others (e.g., Rajendran and Cook /16/), this study quantifies these effects. Another point is the importance of the thermomechanical variables, as well as the Bauschinger effect, in determining the total time-response of ceramics to high-strain-rate deformation.

The constitutive model presented here is quite easy to implement in a hydrodynamic computer code. Methods have been given to estimate the required parameters when adequate data are not available. The model successfully reproduces a variety of experiments on six ceramics.

In order to improve the model, additional experimental information is needed. The most important are the shear and longitudinal sound speeds vs pressure. Also helpful would be Y-vs-$\dot{e}$ data for B_4C and TiB_2, diamond cell studies of the structural changes in TiB_2, additional Hugoniot data for nonporous samples (particularly SiC, PSZ, and AlN) and additional shock-wave profiles (particularly AlN, and PSZ) at pressures below any phase transformation.

Acknowledgments

I would like to thank Dr. Dennis Grady (Sandia National Laboratories) and Dr. James Lankford (Southwest Research Institute) for making available their unpublished data. I would also like to thank Dr. Michael Guinan and Dr. Gordon Smith (Lawrence Livermore National Laboratory) for their help and advice.

Work performed under the auspices of the U.S. Department of Energy by the Lawrence Livermore National Laboratory under Contract No. W-7405-Eng-48.

References

/1/ Steinberg, D, Cochran, S and Guinan, M, J. Appl. Phys. 51 (1980) 1498.
/2/ Steinberg, D, and Lund, C, J. Appl. Phys. 65 (1989) 1528.
/3/ Cochran, S, and Banner, D, J. Appl. Phys. 48 (1977) 2729.
/4/ Steinberg, D, Computer Studies of the Dynamic Strength of Ceramics. Lawrence Livermore National Laboratory Report UCRL-ID-106004 (1990).
/5/ Guinan, M, and Steinberg, D, J. Phys. Chem. Solids 35 (1974) 1501.
/6/ Wiley, W, Manning, W and Hunter Jr, O, J. Less Common Metals 18 (1969) 149.
/7/ Grady, D, in Mechanics of Geomaterials, edited by Bazant, Z (Wiley, 1985), p. 129.
/8/ Grady, D, J. Mech. Phys. Solids 36 (1988) 353.
/9/ Lankford, J, J. Mat. Sci. 18 (1983) 1666.
/10/ Lankford, J, J. Mat. Sci. 20 (1985) 53.
/11/ Lankford, J, Anderson, C and Walker, J, Study of Compressive Strength Behavior of Ceramic Materials. Southwest Research Institute Report for Project 06-2404 (1989).
/10/ Lankford, J, J. Mat. Sci. 20 (1985) 53.
/12/ Kipp, M, and Grady, D, Shock Compression and Release in High-Strength Ceramics. Sandia National Laboratories Report SAND89-1461, UC-704 (1989).
/13/ Gust, W, and Royce, E, J. Appl. Phys. 42 (1971) 276.
/14/ Emin, D, Physics Today 40(1) (1987) 55.
/15/ Gust, W, Holt, A and Royce, E, J. Appl. Phys. 44 (1973) 550.
/16/ Rajendran, A, and Cook, W, A Comprehensive Review of Modeling of Impact Damage in Ceramics. University of Dayton Research Institute Report AFATL-TR-88-143 (1988)